



DISSIPATION ELEMENT ANALYSIS VIA HIGH-SPEED RAYLEIGH SCATTERING IN A TURBULENT JET FLOW

M. GAMPERT^{1,a}, P. SCHAEFER¹, N. PETERS¹

¹ Institute for Combustion Technology, RWTH Aachen, 52056, Germany

^aCorresponding author: Tel.: +49/241/8094619; Fax: +49/241/8092923; Email: m.gampert@itv.rwth-aachen.de

KEYWORDS:

Main subjects: Scalar turbulence, flow visualization

Fluid: Turbulent round jet flow

Visualization method(s): High-speed Rayleigh scattering

Other keywords: Scalar turbulence, dissipation elements

ABSTRACT: Based on the extreme points of turbulent scalar fields, Wang and Peters (2006, 2008) developed the theory of dissipation elements. Starting from every grid point, trajectories along the ascending and descending gradient directions can be calculated, which inevitably end in extreme points. All points that share the same two ending points define a finite volume called dissipation element, which is parameterized by its linear length l between and the scalar difference $\Delta\theta$ at the extreme points. Based on this theory, space filling and non-arbitrary elements are identified, which allow the reconstruction of statistical properties of the field as a whole in terms of conditional statistics within the elements. In the present study, a turbulent round propane jet discharging from a nozzle with diameter $d=12\text{mm}$ into surrounding CO_2 has been chosen as the core of the experimental set-up. The free shear flow, i.e. the mixture fraction of propane and CO_2 , is visualized via Rayleigh scattering of a diode pumped double cavity Nd:YLF laser at the molecules. As we need a three-dimensional test section, in which dissipation elements can be identified, a laser sheet is used to illuminate a two-dimensional plane perpendicular to the jet axis. The resulting signal is recorded with a high speed CMOS camera. In a next step, the recorded time series of the planar test section at a fixed downstream position is transformed into a spatial signal based on Taylor's hypothesis so that we obtain a frozen three-dimensional volume of the mixture fraction field. The latter can be post-processed using the same algorithms as for the DNS and yields a good agreement of the statistical properties of dissipation elements on the one hand and allow their visualization on the other hand.

INTRODUCTION: One of the many approaches in turbulence research is to study geometrical structures or characteristic points in the flow field, which allow the extraction of representative information to describe and statistically reconstruct the whole field. [1] analyzed the behavior at the smallest scales of turbulent scalar fields in terms of the properties of zero gradient points and minimal gradient surfaces. He concluded that these regions of the field are of physical importance to the problem of turbulent mixing. Based on the extreme points of turbulent scalar fields, i.e. points of vanishing scalar gradient, [2, 3] developed the theory of dissipation elements, which arise as natural geometries in turbulent scalar fields, when these are analyzed by means of gradient trajectories. Starting from every grid point, trajectories along the ascending and descending gradient directions can be calculated, which inevitably end in extreme points. All points that share the same two ending points define a finite volume which is called a dissipation element. These elements are parameterized by two values, namely the linear length l between and the scalar difference $\Delta\theta$ at the extreme points.

Based on this theory, space filling and non-arbitrary elements are identified, which allow the reconstruction of statistical properties of the field as a whole in terms of conditional statistics within the elements. Examples of such analysis can be found in [4-6]. In addition, the latter work analyzed dissipation elements numerically in five different flow types and confirmed the theoretically predicted independence of the normalized pdf of the length of dissipation elements from Reynolds number and type of turbulent flow. From the definition of dissipation elements it follows that their



temporal evolution in turbulent fields is inherently connected to the evolution of their ending points, which are separated by a mean linear distance l_m of the order of the Taylor microscale λ , see [2]. In addition, direct numerical simulations of homogeneous shear turbulence revealed that a resolution of the order of the Kolmogorov scale η is needed to obtain grid independent statistics. As dissipation elements have mostly been analyzed in simulations so far, a detailed experimental verification is desirable. Due to their corrugated three-dimensional geometry in combination with the required resolution, such an experimental validation is challenging. For a first attempt using three-dimensional measurements of the velocity field in a channel flow obtained via tomographic PIV see [7].

We study dissipation elements in a passive scalar field θ , which is governed by the convection-diffusion equation

$$\partial\theta/\partial t + u_i(\partial\theta/\partial x_i) = D \partial^2\theta/\partial x_i^2,$$

where D is the diffusion coefficient and u_i denotes the velocity component in i -direction, while repeated indices imply summation. A wide range of experimental investigations of such a scalar field can be found in the literature, three-dimensional data however is limited as often single- or multi-point measurements in combination with Taylor's hypothesis are conducted, see for instance [8,9], which for obvious reasons are of limited use in the context of dissipation element analysis. The development of advanced laser optical techniques with a high pulse energy at a high repetition rate has facilitated the experimental investigation of spatially three-dimensional conserved scalar quantities. In such measurements, the three-dimensional information is found either by imaging in parallel, spatially distinct two-dimensional planes or via a sweeping of a single two-dimensional laser sheet in sheet normal direction, see for instance [10] for an overview. For the present purpose however, both approaches are impractical as in the first one the minimal distance, i.e. the maximal resolution, is limited by the minimal distance between the two planes at which the signals do not interfere. This restriction is not only of importance for the analysis of dissipation elements, but also creates a severe restriction, when three-dimensional gradient quantities in scalar turbulence such as the scalar dissipation rate χ are considered. The latter is for any dynamically passive, conserved scalar θ defined as the scalar gradient magnitude squared times the diffusion coefficient D , yielding

$$\chi = 2D(\partial\theta/\partial x_i)^2 = 2D[(\partial\theta/\partial x)^2 + (\partial\theta/\partial y)^2 + (\partial\theta/\partial z)^2].$$

The second approach has successfully been used for measurements in water, see for instance [11], but proves to be difficult in the gas-phase as the Schmidt number $Sc (= \nu/D, \text{ where } \nu \text{ is the kinematic viscosity})$, is in liquids roughly three orders of magnitude larger than in the gas-phase. In the next section, we will therefore present a method, which combines a high-speed Rayleigh scattering technique with Taylor's hypothesis to resolve the Kolmogorov scale η in all three spatial directions, though at moderate Reynolds numbers $Re_\lambda (= u \lambda/\nu, \text{ where } u \text{ denotes the longitudinal r.m.s. velocity})$. In section three, we present results for the distribution of extreme points in a scalar field, their mean distance as well as an investigation of the spatial decomposition of the field using dissipation elements, before the paper is concluded in section four.

EXPERIMENT: The experiments were performed in a co-flowing turbulent jet facility in the Institute for Combustion Technology at RWTH Aachen. Figure 1 shows the schematic of the experimental setup. The facility consists of a center tube made of steel with an inner diameter of 12 mm. The surrounding co-flow tube had a diameter of 150 mm, which was large enough to reduce the experimental setup to a two-stream problem. Research grade propane (99.95% pure) was fed through the center tube using a flow controller (OMEGA FMA-2600A) at various flow rates to achieve the desired Reynolds number. The co-flow gas was chosen as carbon dioxide owing to its larger Rayleigh cross-section, which was necessary to obtain an accurate determination of the scalar superlayer. For the different experimental runs, the mean velocity of CO_2 was 0.05 m/s. Table 1 shows the flow configurations of all the experimental runs made in this work. The Reynolds number Re_D based on jet exit conditions, was varied between 3,000 and 18,440 and the corresponding jet exit velocity was between 1.15 and 7.1 m/s. Furthermore, $Re_\lambda (= u_{rms} \lambda / \nu_{ci})$ shown in the table, is the local Taylor based Reynolds number on the center line. As different measurements have been performed at a fixed axial



position with different jet exit velocities, we will refer to them in the following for instance with $x/d=20-1/-2/...$ with increasing Reynolds number Re_D .

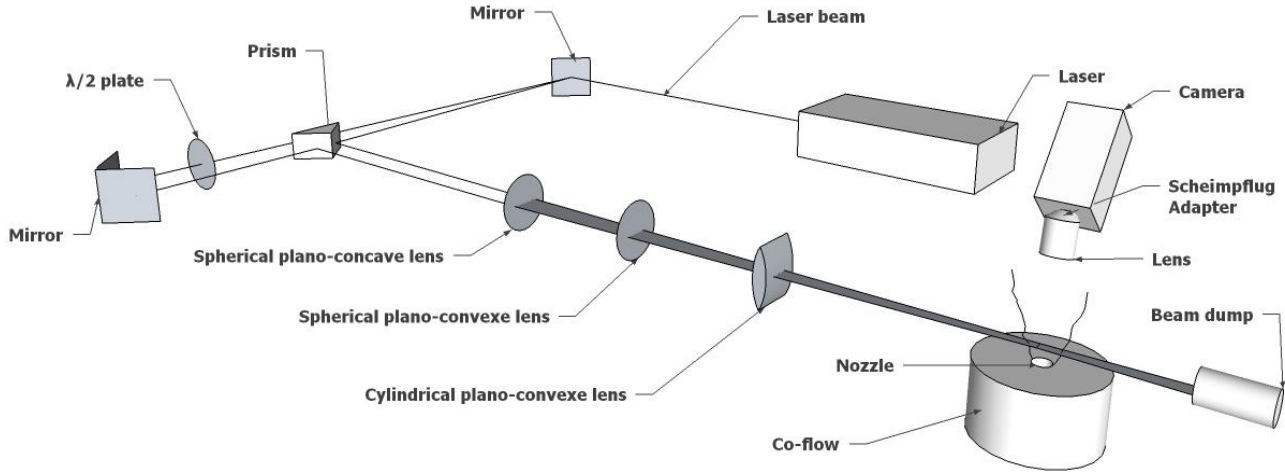


Figure 1: Experimental setup

The objective of the experiments was to obtain spatially resolved scalar field images, which were acquired using high-speed two-dimensional Rayleigh scattering imaging to examine the statistics of the scalar superlayer. To this end, two frequency doubled beams ($\lambda = 527$ nm) from a high-frequency dual-head Nd:YLF laser were combined to deliver an energy of about 32 mJ/p at 1 kHz (32 W). The polarization of both of the beams was normal to the jet axis which maximized the Rayleigh scattering signals from the radial-azimuthal plane. The beams were transformed into a horizontal collimated sheet using a combination of a Galilean telescope (expansion ratio of 1.5) and a cylindrical lens. The width and the thickness (FWHM) of the resultant sheet were approximately 10 mm and 0.3 mm respectively. Images were acquired at 1 kHz using a high-speed CMOS camera (LaVision HighSpeedStar 6) fitted with a camera lens (Nikon f.l. = 85 mm) stopped at f/1.4. An extension ring of 20 mm length was placed between the camera and the lens to minimize the working distance; the resulting field of view is about 60 mm X 60 mm.

Case	10-1	10-2	15-1	15-2	20-1	20-2	30
x/d	10	10	15	15	20	20	30
U_j[m/s]	1.15	2.26	1.72	3.30	1.82	3.30	3.30
U_{cl}[m/s]	0.57	1.10	0.61	1.13	0.50	0.90	0.62
r_{1/2}[mm]	15.31	15.31	21.31	21.31	27.31	27.31	39.31
η[mm]	0.18	0.11	0.20	0.12	0.26	0.16	0.24
λ[mm]	2.30	1.97	3.32	2.20	4.26	3.16	4.61
v_{cl}[m²/s]	6.5×10 ⁻⁶	6.5×10 ⁻⁶	6.95×10 ⁻⁶	6.95×10 ⁻⁶	7.4×10 ⁻⁶	7.4×10 ⁻⁶	7.5×10 ⁻⁶
Re_D	3,000	5,900	4,500	8,610	4,748	8,610	8,610
Re_λ	61	83	72	91	71	96	96

Table 1: Experimental data



The signal-to noise ratio (SNR) in the pure CO₂ region was over 20 and that in the pure propane region over 40. The time interval between the successive images was 1 ms, while the in-plane resolution was 100 microns. This resolution is of the order of the Kolmogorov scale η . The images were recorded using commercial software (LaVision 7.2) and were further processed using computer codes written in-house.

The major sources of systematic uncertainties are the departure from linearity of the camera response and the presence of noise in both propane and CO₂ streams. The departure from the linearity of the camera response is within 4%, as quoted by the manufacturer. The image noise was minimized using an optimal filter designed for the propane stream, so that the scalar spectrum follows Pope's model. However, there is residual noise left in the CO₂, after applying the optimal filter, which induces uncertainty in the determination of the superlayer. The combined uncertainty arising from these sources is estimated to be below 5%.

RESULTS: In the course of this chapter, we will analyze the experimental results with respect to the distribution of extremal points in the measured scalar fields and the scaling of their distance. Then we perform a dissipation element analysis for visualization purposes as well as for a statistical analysis. All analyses in this chapter are based on three independent datasets each comprising 5,400 consecutive images at the various experimental conditions given in table 1.

Investigation of extremal points in scalar fields: In chapter one it has been described briefly that dissipation elements are defined by the spatial region containing all points from which gradient trajectories reach the same two extrema as ending points. In a first step, we therefore examine the distribution of maxima and minima (red and blue points respectively) in the measurement volume. Figure 2 (left) depicts these points in only a smaller part of the box to facilitate visibility of the structure.

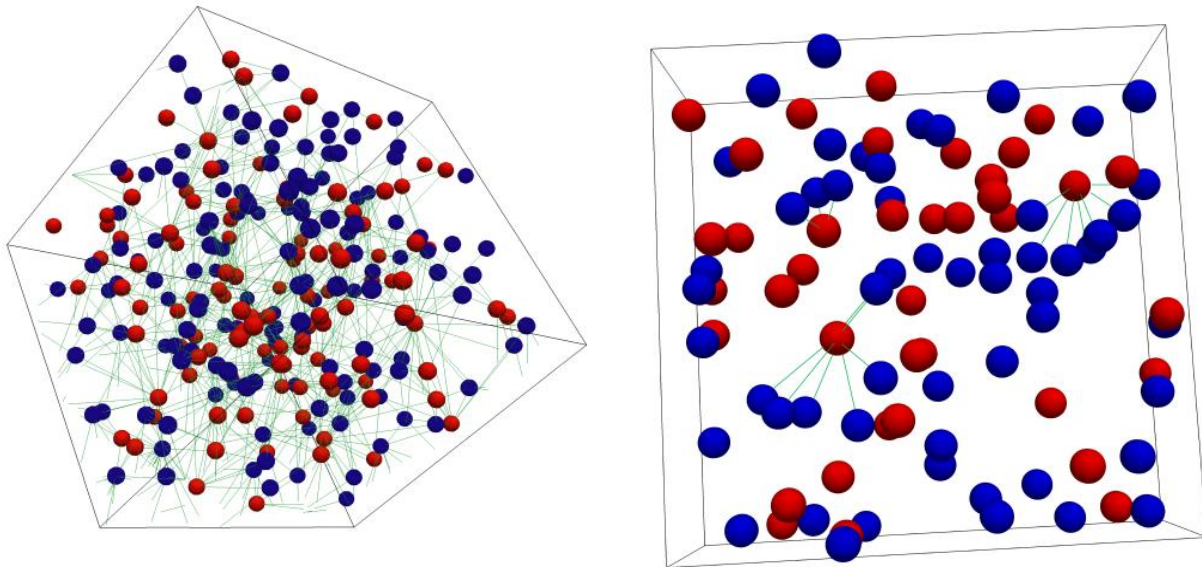


Figure 2: Distribution of extremal points in a section of the box (left). Blue points are minima and red points are maxima, which are connected by straight green lines for each dissipation element. (right) Illustration of secondary splitting.

Overall, we observe approximately an equal number of maximum and minimum points, though we find slightly more minima than maxima. For each dissipation element the two ending points have been connected by a straight green line. In addition, we show a zoom into a small fraction of the box in figure 2 (right), where we observe strings of minimum points indicated by the connecting line to their mutual maximum point. [1] has analyzed the behavior at the smallest scales of turbulent scalar fields in terms of the properties of zero gradient points and minimal gradient surfaces. Among



other findings, he identified two physical mechanisms which lead to the creation of new zero gradient points. While initially zero gradient points must be created from regions of uniform scalar gradient, he concludes that the majority of such points results from the combined action of strain and diffusion on existing zero gradient points. This leads to their splitting into new extreme points, which he called secondary splitting. [2] already reported this effect in regions of large strain rates using DNS of homogenous shear turbulence and attributed it to the physical effect of secondary splitting. This multiplication of extremal points due to secondary splitting may also be responsible for the corrugated shape of many dissipation elements, see [5] for further analyses.

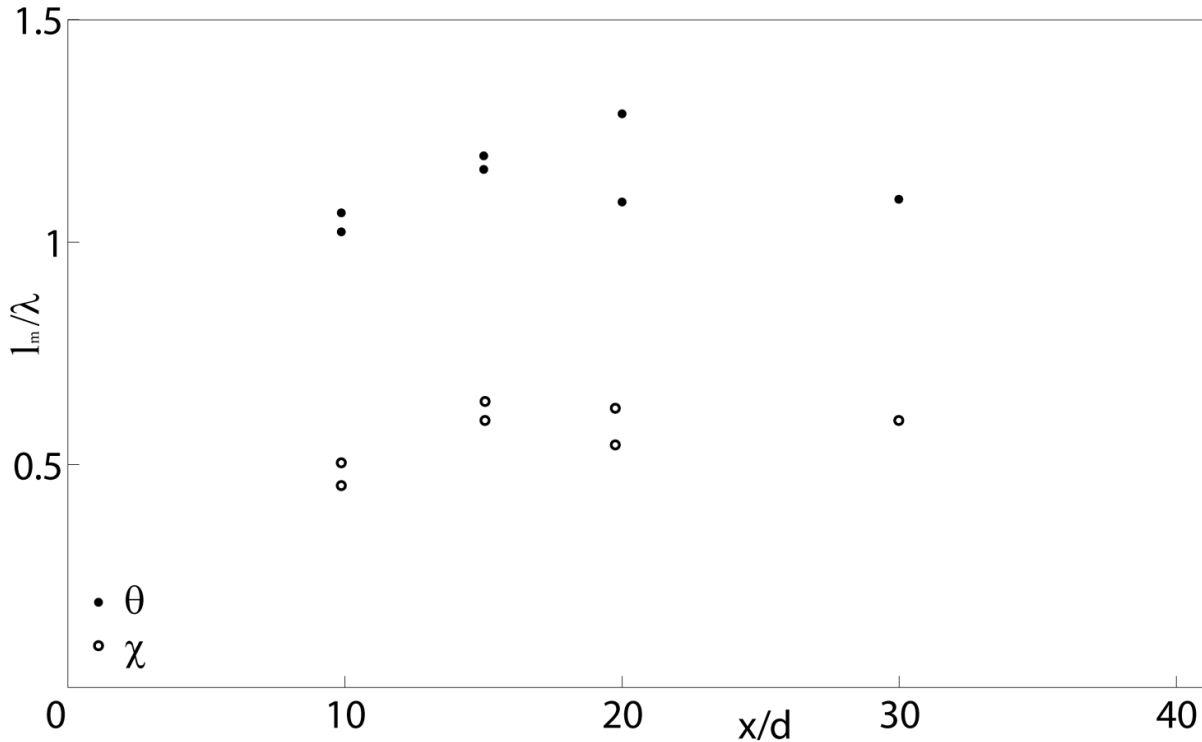


Figure 3: The ratio between the mean linear distance to the Taylor microscale l_m/λ for the mass fraction field denoted by θ and the scalar dissipation field denoted by χ as a function of the downstream position x/d .

[2, 3] and [6] investigated the scaling of the mean linear distance l_m between two extreme points using DNS of various turbulent flows and scalar fields. The authors conclude that the mean linear separation length of extreme points is of the order of the Taylor scale of the velocity field defined as

$$\lambda_v = (10 \nu k / \epsilon)^{1/2}$$

in which k denotes the turbulent kinetic energy and ϵ is the energy dissipation. Based on their analysis, it can also be concluded that only extreme points with a large separation length are subject to secondary splitting, while for small separations diffusive processes become dominant, which lead to a mutual annihilation of the extreme points. For the general case of arbitrary Schmidt numbers, [1] concluded that the separation distance of extreme points scales as

$$l_m \propto (D/\gamma)^{1/2}$$

where γ denotes the root mean square rate of strain, a scaling which coincides with the scaling proportional to the Taylor length found by [3] for unity Schmidt numbers. Figure 3 shows the ratio of the mean linear distance to the Taylor micro-scale over the nozzle distance for the different measurements and the fields of θ and χ . The afore discussed proportionality is clearly illustrated as $l_m/\lambda \approx 1$ for θ independent of the measurement location x/d . The same



observation is valid for the χ field, where the constant value of the ratio lies at around $l_m/\lambda \approx 0.6$. As will be discussed below, this lower value is no surprise due to the shorter distance between two extreme points in the field of the scalar dissipation rate. This scaling of the mean distance between extreme points with the Taylor microscale is also found for other critical points: [12] showed that the average distance between neighboring stagnation points is proportional to λ using the generalized Rice theorem.

Furthermore, this scaling of the mean linear distance between maximum and minimum points can be related on dimensional grounds to the number density of extreme points via $n_{ex} \propto l_m^{-3}$. Combining the latter proportionality and the results displayed in figure 3, we can further state $n_{ex} \propto \lambda^{-3}$ a finding which is of particular interest, as a similar scaling has been obtained by [13] for the number density n_s of stagnation points. They concluded $n_s \approx C_s L^{-3} (L/\eta)^{D_s}$, where C_s is a dimensionless number and $D_s=2$ can be interpreted as a fractal dimension. Introducing the relation between η , λ and L , one obtains $n_s \propto \lambda^{-3}$, which equals the scaling of the number density of extreme points in a scalar field as obtained in the present experimental data. Finally, that many more extremal points are found in the χ -field as compared to the θ -field, indicates the well-known highly intermittent structure of the χ -field, see for instance [9, 14] and [15].

Dissipation element analysis: The motivation for dissipation elements is the reconstruction of the entire scalar field by means of an adequate parameterization of the geometric and scalar properties of the elements. As the linear length is uniquely defined and a more easily accessible parameter than an appropriate average of the curvilinear length, it has been chosen along with $\Delta\theta$ the scalar difference between the extremal points, as the two statistical parameters to describe dissipation elements. As each dissipation element per definition contains one maximum and one minimum point, the scalar extreme points are part of more than one element, i.e. are connected with more than one other extreme point.

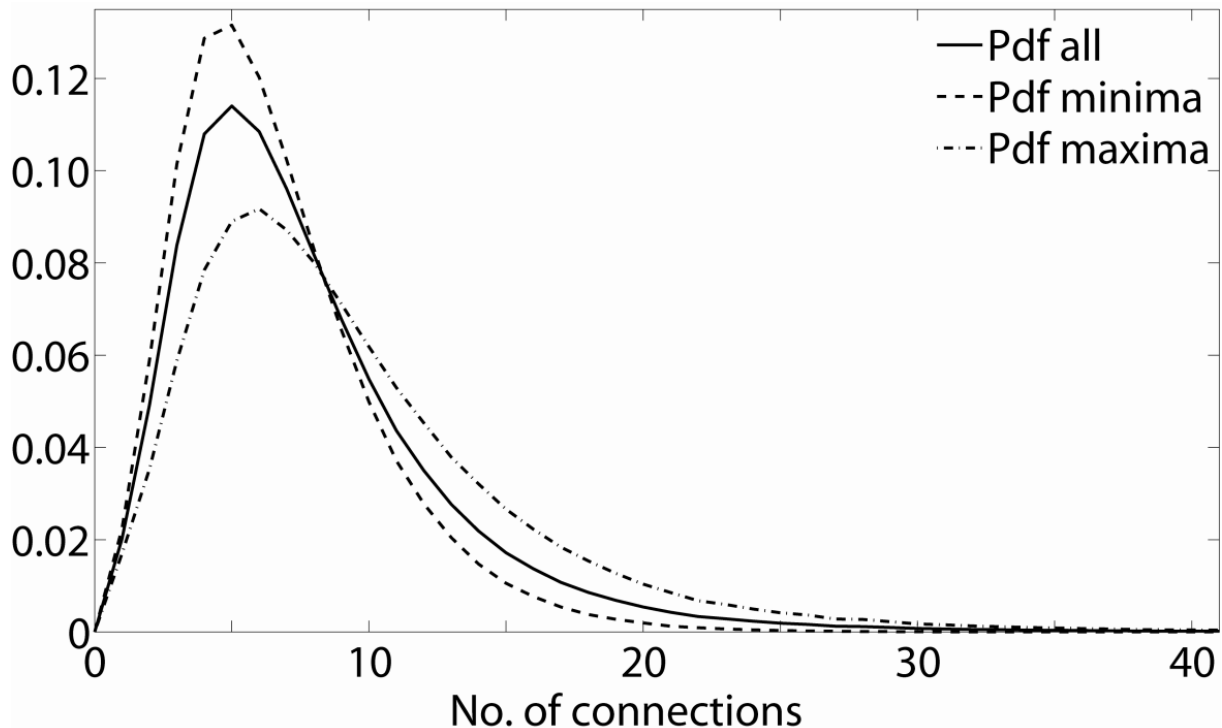


Figure 5: Pdf of the number of connections per extreme point, maximum and minimum.

This number of connections, however, is not constant but rather follows a distribution. The latter is shown in figure 5 for all minimum and maximum points as well as all extreme points in case 30. We find that the number of connections of minimum points is smaller than the one of maxima. The maximum of the former is at five connected maxima per



minimum point with on average 6.31 connections, while it is located for the latter at six connections with an average of 8.41. Overall, however, we find 7.32 connections per extreme point with a maximum probability of five connections. These values vary only negligibly between the different cases.

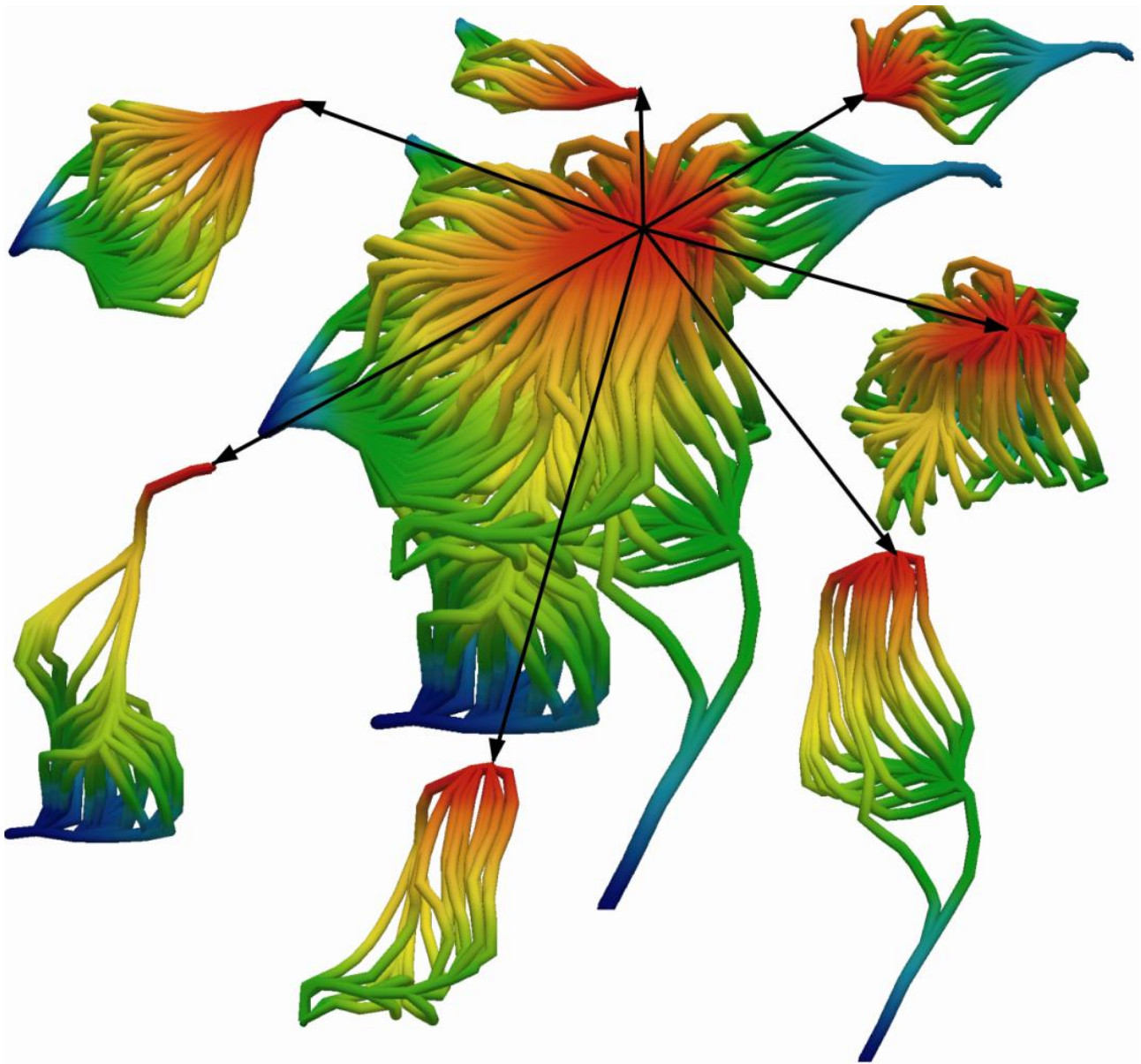


Figure 4: Example of seven dissipation elements based on the concentration field θ sharing the same maximum. The scalar value increases from the minimum points (blue) to the maximum (red).

The inter-twisted nature in of dissipation elements is illustrated in figure 4, where all dissipation elements which share one maximum are shown. As one can observe, there are seven elements, which are space-filling, strongly vary in shape and are connected via the same maximum point.

Further examples for the elements as obtained from various measurements of the θ -field are displayed in figure 6. One can observe that experimentally obtained dissipation elements have the same convoluted, irregular and corrugated shape

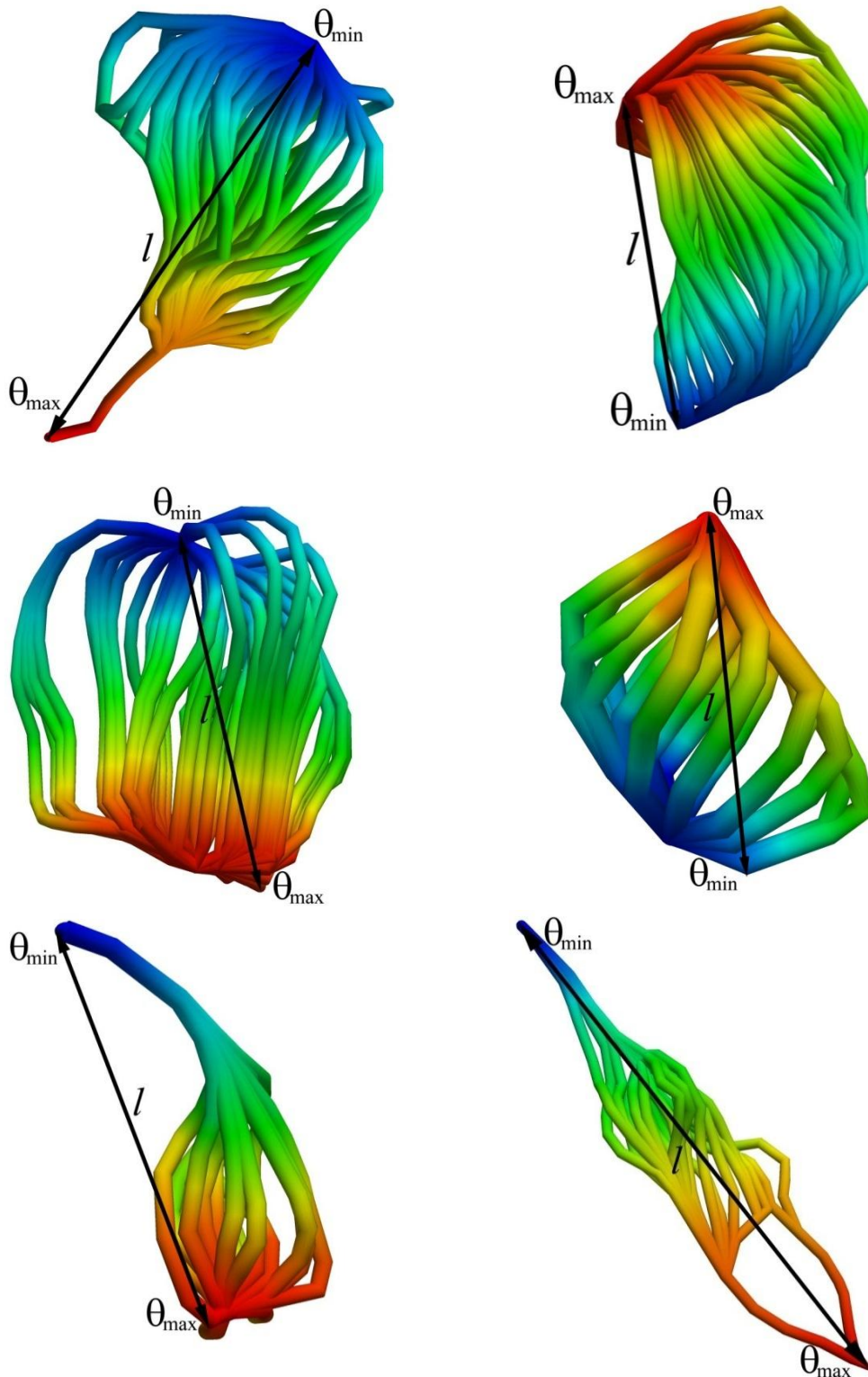


Figure 6: Examples of dissipation elements calculated from the concentration field θ . The scalar value increases from the minimum (blue) to the maximum (red) point.

already known from DNS. As has been discussed in the introduction, the elements are space-filling so that neighboring ones are strongly inter-twisted.



RESULTS: Based on high-speed Rayleigh scattering imaging of a turbulent round propane jet discharging into surrounding CO₂, we have investigated the distribution of scalar extreme points and performed a dissipation element analysis. For the former we observe a mean linear distance which is of the order of the Taylor microscale. This proportionality is of particular interest as it can be translated into a number density of scalar extreme points which resembles the one obtained in [13] for stagnation points. We have then visualized and statistically investigated so called dissipation elements, which are three-dimensional volumes that contain all grid points whose gradient trajectories connect the same two extreme points. The experimental visualization of dissipation elements confirms the inter-twisted and corrugated shapes of these elements which also been observed in DNS. As dissipation elements are space-filling, multiple elements share a minimum and maximum point, respectively. A statistical analysis of the latter property revealed that on average each minimum is shared by only 6.31 elements, while each maximum is part of 8.41 elements, meaning that on average an extreme point is part of 7.32 dissipation elements.

ACKNOWLEDGEMENT: This work was funded by the NRW-Research School "BrenaRo" and the cluster of Excellence "Tailor-Made Fuels from Biomass", which is funded by the Excellence Initiative of the German federal state governments to promote science and research at German universities.

References

1. Gibson C.H. *Fine structure of scalar fields mixed by turbulence i. zero gradient points and minimal gradient surfaces*. Phys. Fluids 1968 **11**, 2305–2315
2. Wang L. & Peters N. *The length scale distribution function of the distance between extremal points in passive scalar turbulence*. J. Fluid Mech. 2006 **554**, 457–475
3. Wang L. & Peters N. *Length scale distribution functions and conditional means for various fields in turbulence*. J. Fluid Mech. 2008 **608**
4. Schaefer P. et al. *Testing of different model equations for the mean dissipation using Kolmogorov flows* Flow. Turbulence and Combustion 2010 **85**, 225–243
5. Schaefer P. et al. *The secondary splitting of zero gradient points in a turbulent scalar Field*. J. Eng. Math. 2011 **71**(1), 81 – 95
6. Gampert M. et al. *Extensive strain along gradient trajectories in the turbulent kinetic energy field*. New J. of Physics 2011 **13**, 043012
7. Schaefer L. et al. *Investigation of dissipation elements in a fully developed turbulent channel flow by tomographic particle-image velocimetry*. Phys. Fluids 2010 **23**, 035106
8. Antonia R.A. et al. *Temperature structure functions in turbulent shear flows*. Physical Review A 1984 **30**, 2704–2707
9. Mydlarski L. & Warhaft Z. *Passive scalar statistics in high-péclet-number grid turbulence*. J. Fluid Mech. 1998 **358**, 135–175
10. Su L.K. & Clemens N.T. *Planar measurements of the full three-dimensional scalar dissipation rate in gas-phase turbulent flows*. Exp. Fluids 1999 **27**, 507–521
11. Miller R.J. et al. *Multipoint correlations of concentration fluctuations in a turbulent passive scalar*. Exp Fluids 2008 **44**, 719–732
12. Goto S. & Vassilicos J.C. *The dissipation rate coefficient is not universal and depends on the internal stagnation point structure*. Phys. Fluids 2009 **21**, 035104
13. Vassilicos J.C. & Dávila J. *Richardson's Pair Diffusion and the Stagnation Point Structure of Turbulence* Phys. Rev. Letters 2003 **91**, 14
14. Sreenivasan K.R. & Antonia R.A. *The phenomenology of small-scale turbulence*. Annu. Rev. Fluid Mech. 1997 **29**, 435–472
15. Vedula P. et al. *Dynamics of scalar dissipation in isotropic turbulence: a numerical and modelling study*. J. Fluid Mech. 2001 **433**, 29–60